



This is a post-refereeing final draft. When citing, please refer to the published version:

Concialdi, P., Di Prima, S., Bhanderi, H.M., Stewart, R.D., Abou Najm, M.R., Lal Gaur, M., Angulo-Jaramillo, R., Lassabatere, L., 2020. An open-source instrumentation package for intensive soil hydraulic characterization. *Journal of Hydrology* 582. <https://doi.org/10.1016/j.jhydrol.2019.124492>



An open-source instrumentation package for intensive soil hydraulic characterization

Paola Concialdi ¹, Simone Di Prima ^{2,3,*}, Harsh M. Bhanderi ⁴, Ryan D. Stewart ⁵, Majdi R. Abou Najm ⁶, Murari Lal Gaur ⁴, Rafael Angulo-Jaramillo ² and Laurent Lassabatere ²

¹ University of Palermo, Department of Agricultural, Food and Forest Sciences, Palermo, Italy.

² Université de Lyon; UMR5023 Ecologie des Hydrosystèmes Naturels et Anthropisés, CNRS, ENTPE, Université Lyon 1, Vaulx-en-Velin, France.

³ University of Sassari, Department of Agricultural Sciences, Sassari, Italy.

⁴ College of Agricultural Engineering, Anand Agricultural University, Godhra, Gujarat, India.

⁵ School of Plant and Environmental Sciences, Virginia Polytechnic Institute and State University, Blacksburg, VA, United States.

⁶ Department of Land, Air and Water Resources, University of California, Davis, CA 95616, United States.

* Corresponding Author. E-mail: sdiprima@uniss.it

Abstract

We present a new open-source and modular instrumentation package composed of up to ten automatic infiltrometers connected to data acquisition systems for automatic recording of multiple infiltration experiments. The infiltrometers are equipped with differential transducers to monitor water level changes in a Mariotte reservoir, and, in turn, to quantify water infiltration rates. The data acquisition systems consist of low-cost components and operate on the open-source microcontroller platform Arduino. The devices were tested both in the laboratory and on different urban and agricultural soils in France and India. More specifically, we tested three procedures to treat the transducers readings, including a filtering algorithm that substantially improved the ability to determine cumulative infiltration from raw data. We combined these three procedures with four methods for estimating the soil parameters from infiltrometer data, showing pros and cons of each scenario. We also demonstrated advantages in using the automatic infiltrometers when infiltration measurements were hindered by: i) linearity in cumulative infiltration curves owing to gravity-driven flow, ii) an imprecise description of the transient state of infiltration, and iii) the occurrence of soil water repellency. The use of the automatic infiltrometers allows the user to obtain more accurate estimates of soil hydraulic parameters, while also reducing the amount of effort needed to run multiple experiments.

Keywords: automatic infiltrometer; infiltration rate measurements; soil hydraulic properties; Arduino.

1. Introduction

Different automated devices have been developed to measure water infiltration rates in the field. Automation strategies have involved the use of many different set-ups and sensors, including pressure transducers (e.g., Ankeny et al., 1988; Casey and Derby, 2002; Constantz and Murphy, 1987; Di Prima, 2015; Madsen and Chandler, 2007; Prieksat et al., 1992), infrared sensor systems (Milla and Kish, 2006), micro flow-meters (Moret-Fernández et al., 2012), reflectometry probes (Moret et al., 2004), and load cell sensors (Klípa et al., 2015; Zumr et al., 2019). Among these approaches, pressure transducers are widely used for field applications given their simplicity of use and low price. These sensors allow the user to monitor water level changes in a Mariotte reservoir, and, in turn, to quantify water infiltration rates. Automation of a Mariotte reservoir was firstly proposed by Constantz and Murphy (1987). These authors used a pressure transducer connected at the top of a Mariotte reservoir to monitor the head-space tension during the drop of the water level. This technique was used by Ankeny et al. (1988) to automate a tension infiltrometer for infiltration rates measurements under negative suction. These authors tested two different set-ups: the first configuration had a single pressure transducer located at the top of the Mariotte reservoir, while the second configuration added another pressure transducer at the base of the water

column. The use of two transducers overcame some of the difficulties generated from the tension fluctuations caused by bubbling. This strategy was further improved by Casey and Derby (2002), who used a differential transducer with two ports to automate an SW-080B tension infiltrometer, and Madsen and Chandler (2007), who automated a mini-disk infiltrometer (Decagon, 2014) using pressure transducers. Selker et al. (2009) incorporated pressure transducers and pneumatic reed switches to create a tension infiltrometer with automated, near-instantaneous control over the tension applied to the water source. Pressure transducers have also been used to automate single-ring infiltrometers (Prieksat et al., 1992).

The single-ring infiltrometer technique (Reynolds and Elrick, 1990) is a widespread method (e.g., Braud et al., 2017), which has the advantages of speed and simplicity over more cumbersome procedures for performing field-saturated soil hydraulic conductivity measurements, such as the Guelph permeameter and the double-ring infiltrometer (Di Prima et al., 2019). These infiltrometers maintain a quasi-constant head in a containment ring, allowing to calculate infiltration rates under ponding conditions (Angulo-Jaramillo et al., 2016). Recently, Di Prima (2015) presented a new automated single-ring infiltrometer. This device is equipped with a differential transducer to measure the stepwise drop of water level in a Mariotte reservoir. The data acquisition system consists of low-

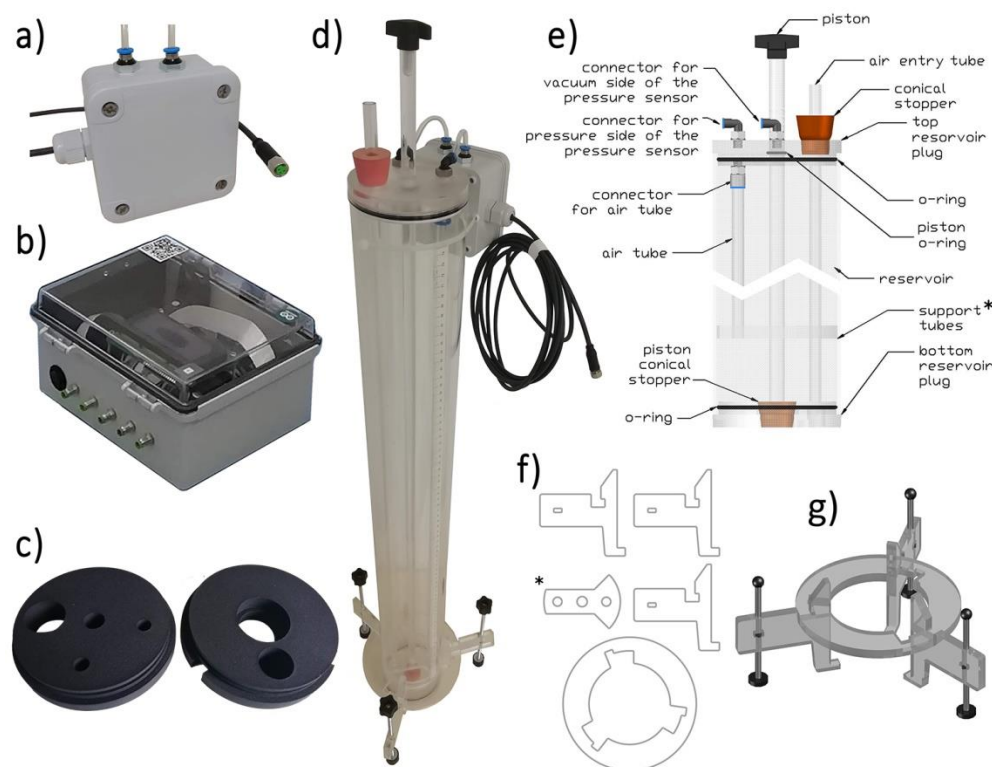


Figure 1. Main components of the automatic system. (a) Box with differential pressure sensor MPXV5010DP; (b) data acquisition system with Arduino MEGA 2560 Rev3; (c) 3D printed top and bottom plugs realized by Multi Jet Fusion (MJF) printing technology; (d) Infiltrometer; (e) detailed scheme of the infiltrometer; (f) laser cutting project for the realization of the (g) tripod and (*) support tubes. The project files for the manufacture of the plugs and the tripod can be downloaded from the website bestsoilhydro.net.

cost components and uses the open-source Arduino microcontroller platform.

The potential of this automated infiltrometer to reliably derive saturated hydraulic conductivity, K_s , and sorptivity, S , was tested by using three existing BEST algorithms, i.e., BEST-slope (Lassabatere et al., 2006), BEST-intercept (Yilmaz et al., 2010) and BEST-steady (Bagarello et al., 2014). This approach demonstrated that the total volume applied with the prototype version of the infiltrometer (130 mm) may not be sufficient to evaluate steady state conditions, compromising the reliability of the estimates in some cases (e.g., loamy soil). The importance to collect an appropriate number of data points during the transient state was investigated, using analytically generated data, by increasing the precision of the collected information, namely decreasing the cumulative infiltration interval from 5 mm to 2.5 mm. In the case of readings every 2.5 mm, the number of points used to describe the same curve doubled and generated enough points to accurately model the transient state of infiltration. Based on these results, Di Prima et al. (2016) proposed guidelines for the optimization of the design in terms of capacity of the Mariotte reservoir (which affects the cumulative amount of infiltration that can be measured) and the radius of air entry tube (which affects the increment size between two successive measurements). These guidelines thus suggest ways to optimize infiltrimeters to accurately measure transient and steady-state infiltration conditions, yet the actual effectiveness of these improvements have not been assessed using experimental data.

Another limitation on the use of the initial prototype is the need to filter raw data recorded by the transducer. The transducer readings produce a step-shaped or stair-like relationship between time and recorded voltage. These artifacts tend to be caused by air bubble formation in the Mariotte system, and the magnitude and rate of change of the resulting steps tend to depend on the infiltrimeter set-up. Di Prima (2015) and Di Prima et al. (2016; 2017) manually processed the data, which complicated post-processing step and required a

tremendous amount of work and time to determine cumulative infiltration curves. While previous work has attempted to ease the analysis of infiltration data from automated infiltrimeters, for instance using the FLOWDATA software developed by Ankeny et al. (1993), such methods are not able to filter out “stair-like” relationships that are often obtained with the proposed infiltrimeter.

Lastly, previous studies have shown that the strong spatial variability of hydraulic properties and water infiltration at the field scale may affect measurement of water cumulative infiltration and related estimates for hydraulic parameters (e.g., Zimmermann et al., 2008). For instance, Lassabatere et al. (2019a) developed the concept of the BMR (Beerkan Multi Run) showing the need for a large dataset of experimental data for a proper representation of the average response and its variability. Automated infiltrimeters may be used to collect simultaneous measurements at multiple locations for relatively long periods of time, thus providing accurate data at high spatial and temporal resolutions. The use of automated infiltrimeters may therefore improve characterization of spatial variability in soil hydraulic characteristics, making it important to develop a system that can collect and integrate measurements from multiple units.

In this investigation we present a new modular instrumentation package, based on the original design of Di Prima (2015), that has been updated to include up to ten automatic infiltrimeters for automatic recording of simultaneous infiltration experiments. Following the guidelines in Di Prima et al. (2016), we improved the design of the devices in terms of reservoir capacity to ensure steady state at the end of the experiment, accuracy of the description of the transient phase of the infiltration process, and number of infiltrimeters that can be simultaneously operated. This set of new devices should produce an optimum description of the cumulative infiltration for an optimum hydraulic characterization. The main objectives of this paper were to: i) testing the potential of the instrumentation package to automatically collect data from

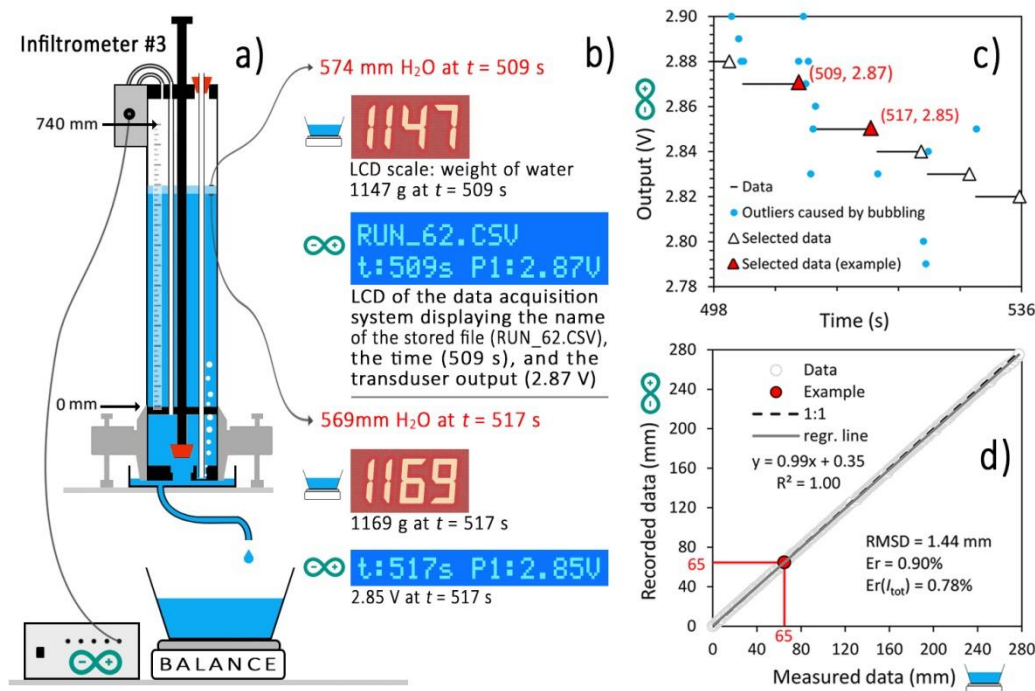


Figure 2. (a) Sketch of the testing procedure; (b) weight of the discharged water and transducer output at time immediately preceding two consecutive bubbling events; (c) manual selection of data at the end of the constant height stages in Mariotte bottle; and (d) comparison between recorded and measured cumulative flow data. Note that the recorded data in subpanel d were firstly converted into water column heights using the calibration function for Infiltrometer #3, and then used to estimate infiltration amounts.

multiple infiltrimeters working simultaneously, ii) improving the treatment of the raw data recorded by the transducers, iii) assessing the use of the infiltrimeters in conjunction with different methods for estimating the soil parameters from infiltrimeter data, and iv) evaluating instrument performance under specific and challenging field conditions, such as highly permeable, slightly sorptive and water repellent conditions.

2. Material and methods

2.1. Improved Infiltrimeter design

The main components of the complete system are illustrated in Figure 1. Each infiltrimeter consists of a Mariotte bottle with a 94-mm inner diameter and a height of 850 mm, with effective water storage height of 740 mm. It provides the capacity to hold the volume of water corresponding to a total cumulative infiltration of 280 mm based on a 150 mm infiltration ring diameter. This water volume represents 150 mm of additional water available for infiltration compared to the prototype proposed by Di Prima (2015).

An air entry tube is positioned with its lower end at short distance from the reservoir base, which controls the air entry in the Mariotte bottle and thus the water level inside the ring. The air entry tube has a 7 mm inner diameter, compared to the 6.5 mm inner diameter used in the original prototype. Using this larger diameter tube changed the cumulative infiltration interval from ~4.5 mm in the original prototype to ~2 mm in the updated version (see section 3.3). This change was implemented with the goals of increasing the precision of the collected information and allowing the collection of many data points during the first stage of the process.

The Mariotte bottle is closed by a top and a bottom plug (Figure 1c-e) and sustained through a tripod (Figure 1f-g) made of four interlocking parts (3 legs and 1 circular support). The design of the tripod allows the user to easily regulate the distance between the base of the infiltrimeter and the infiltration surface, with an adjustable range from 2-3 mm at the closest setting up to 90 mm at the most distant setting. The tripod components were manufactured through an online laser

cutting service. This type of service is offered by a number of online companies, which typically allow users to choose the thickness and the type of material and then upload a file (e.g., .eps, .svg or .dxf) that specifies the cutting lines. An illustration of the cutting lines is provided in Figure 1f. The plugs can be realized by different 3D printing technologies, such as stereolithography (SLA), selective laser sintering (SLS), and Multi Jet Fusion (MJF). The project files for the realization of the plugs (Figure 1c) and the tripod (Figure 1f) can be downloaded from the website bestsoilhydro.net. We note that online manufacturer services tend to be cost-effective, allowing the user to build the system for relatively low cost.

2.2. Data acquisition system and differential pressure sensor

The core of the data acquisition system consists of an Arduino Mega microcontroller board, an Arduino wireless shield with an onboard micro-SD socket and a LCD module shield (20 columns and 4 rows) and a differential pressure transducer. The list of components and the Arduino code can be downloaded from the website bestsoilhydro.net. The LCD module requires that a specific library (LiquidCrystal_I2C) be installed into the Arduino IDE; this library can be downloaded from the website wiki.sunfounder.cc. The data acquisition system (Figure 1b) is connected to differential pressure sensors (Figure 1a) using 3-m-long cables. Each system simultaneously connects to as many as five infiltrimeters. The differential pressure sensor box is mounted on the top of the infiltrimeter (Figure 1d). The two ends of the transducer are connected using small plastic flexible tubes (outer diameter = 4 mm) to the head-space of the reservoir and to an acrylic tube (outer diameter = 10 mm, inner diameter = 7 mm, height = 790 mm) descending inside the reservoir. This configuration enables measurement of the pressure difference between the head-space and the bottom of the column of water. The differential pressure transducer used for this application is the piezoresistive differential pressure transducer MPXV5010DP, from NXP semiconductors (nxp.com; other companies that provide similar transducers include SMI and Honeywell). This sensor requires a power

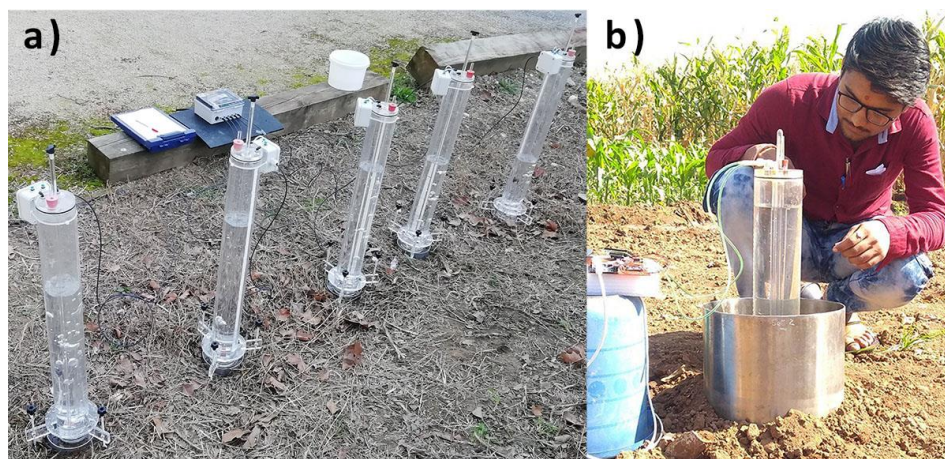


Figure 3. Automated infiltration experiments of the (a) single- and (b) double-ring type carried out respectively at the DOUA site and at the Anand Agricultural University.

supply of 5 V and has an integrated temperature compensation and signal amplification circuit. The transducer provides a linear voltage output for a differential pressure range from 0 to 1000 mm H₂O. The data are recorded on a SD card and simultaneously displayed on the LCD display. The software generates a new comma-separated values (CSV) file every time that the microcontroller is activated. The name of the generated file appears on the LCD.

2.3. Infiltrometer system calibration

Laboratory calibration of the devices was carried out by visually monitoring the height of the water column inside the Mariotte bottle during the complete emptying of the reservoirs. Each infiltrometer was placed within a 150-mm inner diameter cylinder; a quasi-constant water head of 5 mm was maintained inside the cylinder. Visual readings of the water levels were done on a 740-mm long ruler with the zero positioned 10 mm above the bottom end of the tube connected to the pressure side of the differential pressure sensor. Then, a calibration function was created via linear regression between the visual readings of the heights of the water column and the corresponding recorded volts. The calibration function for each infiltrometer was used in subsequent experiments to convert recorded transducer outputs into water column heights, which were then used to estimate infiltration amounts.

2.4. Laboratory testing

All of the infiltrometers were also tested in the laboratory (example shown in Figure 2). Similar to the calibration procedure, the infiltrometer was used to maintain a quasi-constant head of water inside a 150-mm inner diameter cylinder that was connected via an outlet pipe to a collection container set on a balance (Figure 2a). The experiments were carried out by recording the transducer output during the complete emptying of the reservoir while weighing the mass of discharged water (Figure 2a and b). In the example of Infiltrometer #3, the transducer voltage was constant during intervals where bubbles form in the air-entry tube, reflecting a constant water level in the reservoir. Once a bubble reached sufficient size to enter the water column, e.g., at time $t = 509$ s

(observations in Figure 2b and left-most red triangle in Figure 2c), the transducer readings fluctuated and generated easily detectable outliers (blue solid circles in Figure 2c), as already discussed by Ankeny et al. (1988). The transducer readings then stabilized at a constant value until the subsequent bubbling event, e.g., the transducer output stayed at 2.85 V between $t = 510$ and 517 s. As highlighted by Di Prima (2015) and Di Prima et al. (2016), this typically behavior produces a step-shaped relationship between time and recorded voltage (Figure 2c).

2.5. Field testing

After laboratory calibration and testing, we also tested the devices during four experimental campaigns in the field, with three sites in France and one in India. The first two sites (ENTPE-1 and ENTPE-2 sites) are located in the garden of the École Nationale des Travaux Publics de l'État (ENTPE) in the municipality of Vaulx-en-Velin (France). The third site (DOUA site) is a drainage ditch located at the La DOUA scientific campus in the municipality of Villeurbanne (France), which receives runoff mainly originating from adjacent parking lots and sidewalks. These municipalities belong to the Metropolis of Lyon in Auvergne-Rhône-Alpes region in eastern France. The three sites are part of the Lyon city Field Observatory for Urban Water Management (OTHU). The sampled soils ranged in texture from silt to sand (Bouarafa et al., 2019). The fourth experimental site is a sandy loam soil covered by maize crop that is located at the Anand Agricultural University in the western Indian state of Gujarat.

For each site in France, a total of four undisturbed soil cores (50 mm in height and 50 mm in diameter) were collected at randomly sampled points and used to determine both the soil bulk density, ρ_b (g cm⁻³), and the initial volumetric soil water content, θ_i (cm³ cm⁻³) (Table 1).

We used the infiltrometers to carry out a total of fifteen infiltration experiments, with five simultaneous experiments conducted at each French site (Figure 3a). We used stainless steel rings with an inner diameter of 150 mm, inserted shallowly into the soil (~10 mm) according to the Beerkan procedure for single-ring infiltration experiments (Lassabatere et al., 2006).

Table 1. Coordinates, dry soil bulk density, ρ_b (g cm⁻³), and initial volumetric soil water content, θ_i (cm³ cm⁻³) for the three sampled soils in France (sample size for each soil, $N = 4$). Standard deviations are indicated in parentheses.

Site	ENTPE-1	ENTPE-2	DOUA
Coordinates	45°46'42.46"N 4°55'33.68"E	45°46'42.40"N 4°55'30.62"E	45°47'5.67"N 4°52'17.31"E
ρ_b (g cm ⁻³)	1.276 (0.150)	1.280 (0.154)	1.166 (0.043)
θ_i (cm ³ cm ⁻³)	0.378 (0.048)	0.400 (0.057)	0.273 (0.045)

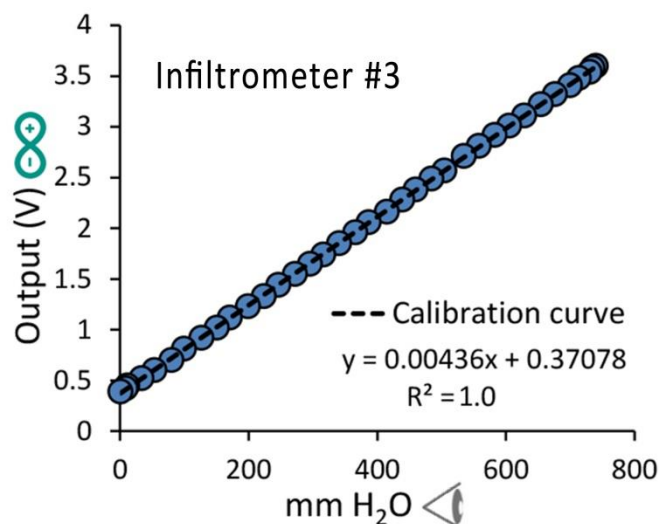


Figure 4. Experimental calibration curve of the MPXV5010DP sensor mounted on Infiltrometer #3. The calibration multiplier is 4.36×10^{-3} V/mm H₂O ($R^2 = 1.0$). (∞) Recorded transducer outputs. (◀) Visual readings of the heights of the water column inside the Mariotte bottle during the complete emptying of the reservoir.

Following the procedure described in Di Prima et al. (2016), we firstly positioned a plastic film on the soil surface inside each ring and applied a small water head of few millimeters (2–3 mm), depending on the surface roughness. The plastic film was also used to minimize disturbance on the soil surface while establishing ponding conditions and to have an accurate data acquisition from the beginning of the run. The infiltrimeters were positioned inside the rings and regulated in height so that the bases were in contact with the ponding water. The Mariotte bottles were filled with tap water and then activated through lifting the pistons. A few seconds after flow began, the data acquisition was started by simply switching on the data acquisition system. Finally, the infiltration experiments started when the plastic films were removed. A video tutorial showing this procedure can be viewed online (Di Prima, 2014). At the ENTPE-1 site, we also used all the automatic infiltrimeters connected to two data acquisition systems for automatic recording of ten simultaneous infiltration experiments. These experiments were aimed to test the potential of the proposed instrumentation package to capture soil heterogeneity.

The hypothesis of an improved description of the cumulative infiltration curve was investigated through a comparison with the prototype proposed by Di Prima (2015). At this aim, we made a comparison between 45 curves collected with the prototype during previous field campaigns (Di Prima, 2015; Di Prima et al., 2017, 2016), and the curves collected with new infiltrimeters at the ENTPE-1, ENTPE-2 and DOUA sites.

At the experimental site in India, we conducted a total of six infiltration experiments. Three runs of the double-ring type were carried out using an inner ring of 150 mm diameter and outer ring of 300 mm diameter. The automatic infiltrimeter was used to maintain constant water depths in the inner rings of 25 mm (Run 1), 50 mm (Run 2), and 75 mm (Run 3), while the

same water depths were maintained in the outer ring manually by pouring the water during the experiments. Assuming that water infiltration below the inner ring was one-dimensional (1D) and that the final steady flow was only gravity driven, we estimated the saturated soil hydraulic conductivity based on the steady infiltration rate (Reynolds et al., 2002). The other three runs used single rings with 150 mm inner diameter. The infiltrimeters were used to maintain constant depths of 25 mm (Run 4), 50 mm (Run 5), and 75 mm (Run 6).

2.6. Treatment of the raw data recorded by the transducers

In this investigation, we propose three different procedures to treat the raw data recorded by the transducer. The first procedure, proposed by Di Prima (2015) and applied by Di Prima et al. (2017; 2016), requires the user to manually select values at the end of the constant height stages, i.e., by sampling the transducer readings at time immediately preceding the bubbling. The second procedure automatically selects these values through an algorithm coded with the open-source software Scilab. The code can be downloaded from the website bestsoilhydro.net. Because the code may fail in certain cases owing to unpredictable noise in the transducer readings, in this investigation we decided to apply both procedures. Further, these two procedures cannot be adopted whenever rapid emptying of the Mariotte bottle causes uninterrupted air bubbling, which may occur during high infiltration rates (Di Prima et al., 2016). Following the suggestion by Di Prima et al. (2016), we therefore applied a third procedure that calculated a moving median to identify the underlying trend of transducer output with time. In the laboratory, the accuracy of these procedures was evaluated through the comparison between recorded and measured cumulative flow data (Figure 2d) in terms of relative error, Er (%), and root mean squared differences, $RMSD$ (mm), defined as:

$$Er = 100 \times \sqrt{\frac{\sum_{i=1}^n (I_i^{exp} - I_i)^2}{\sum_{i=1}^n (I_i^{exp})^2}} \quad (1)$$

$$RMSD = \sqrt{\frac{\sum_{i=1}^n (I_i^{exp} - I_i)^2}{n}} \quad (2)$$

where n is the total number of data pairs, I_i^{exp} (mm) are the measured data, estimated from the mass of discharged water during laboratory tests, and I_i (mm) are the values estimated from the recorded transducer data using the calibration functions. Also, the recorded total cumulative flow, I_{tot} (mm), were compared with the corresponding measured data, I_{tot}^{exp} (mm), using the relative error, $Er(I_{tot})$ (%), defined as follows:

$$Er(I_{tot}) = 100 \times \frac{I_{tot} - I_{tot}^{exp}}{I_{tot}^{exp}} \quad (3)$$

Table 2. Calibration parameters of the ten infiltrimeters.

Infiltrimeter	1	2	3	4	5	6	7	8	9	10
Slope (V/mm H ₂ O)	0.00433	0.00435	0.00436	0.00435	0.00436	0.00433	0.00432	0.00433	0.00436	0.00435
Intercept (V)	0.366	0.346	0.371	0.353	0.354	0.390	0.383	0.347	0.328	0.337
R ²	1.0000	0.9999	0.9999	0.9999	0.9998	0.9999	0.9999	0.9998	0.9998	0.9999

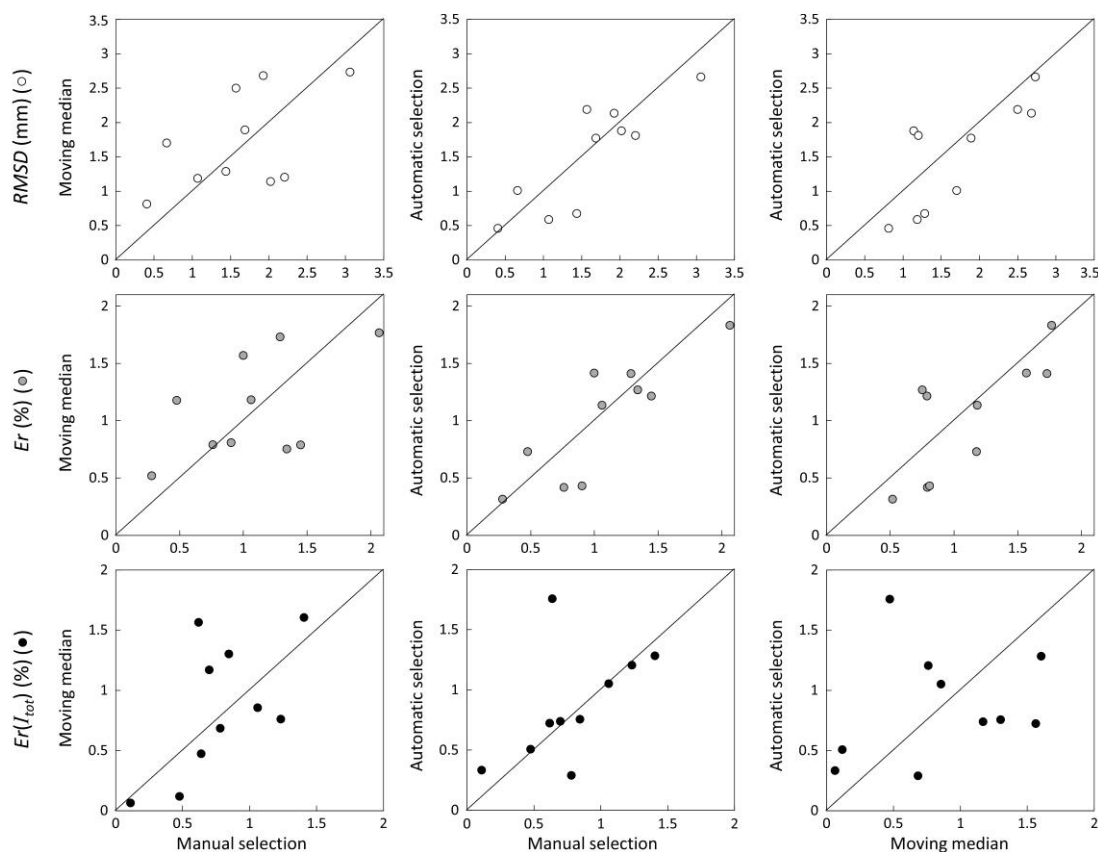


Figure 5. Comparison between the errors obtained from the three procedures used to treat the transducer output.

The three procedures presented above to treat the transducer output (i.e., manual selection, automatic selection and moving median) were subsequently applied to determine the cumulative infiltration curves. In addition, we also considered a fourth procedure described below. According to Angulo-Jaramillo et al. (2016), an expected advantage of the use of the automatic infiltrometers is better accuracy during the transient flow state. In this paper we investigated this hypothesis by processing the raw data in order to obtain “Beerkan-like data”, i.e., cumulative infiltration curves having the same increments (8.5 mm) as manually pouring water volumes into the containment ring. More specifically, the curves obtained by manually sampling the transducer readings were further processed and polynomial regression functions were applied to cumulative data to model the discretized infiltration measurements.

2.7. Estimating hydrodynamic parameters from field experiments

All the cumulative infiltration curves from the four different procedures were subsequently inverted by three different approaches to estimate the soil sorptivity, S ($\text{mm h}^{-0.5}$) and the saturated hydraulic conductivity, K_s (mm h^{-1}). The three approaches represented different algorithms within the Beerkan Estimation of the Soil Transfer parameters (BEST) solution introduced by Lassabatere et al. (2006), Yilmaz et al. (2010), and Bagarello et al. (2014), and differed from one another in the manner by which they fit the experimental cumulative infiltration to the approximate expansion for transient and steady states defined by Haverkamp et al. (1994) and to derive S and K_s . More specifically, BEST-slope (Lassabatere et al., 2006) uses the slope of the straight line defined by the last points (representative of the steady state) to constrain S and K_s , before fitting the transient model to the experimental data by the

optimization of S . BEST-intercept (Yilmaz et al., 2010) uses the intercept of the steady state model to constrain S and K_s , prior fitting the experimental data. Lastly, BEST-steady (Bagarello et al., 2014) uses both the slope and the intercept to resolve a set of two equations (Di Prima et al., 2016), leading to the estimation of the two unknowns, S and K_s . More information on BEST can be found in Angulo-Jaramillo et al. (2019).

K_s values were also estimated using Approach 4 in Stewart and Abou Najm (2018), in which the macroscopic capillary length, λ , was assumed to have a constant value of $\lambda = 150$ mm, following the recommendation of Stewart and Abou Najm (2018). Note that this approach does not require additional information (e.g., particle size distribution, initial and final soil water content and dry soil bulk density) to estimate K_s from infiltration runs. Therefore, it is particularly useful when a large number of locations needs to be sampled, particularly when time and financial resources are limited (Di Prima et al., 2019). At the Indian site, K_s values were estimated using Approach 4, as this method is also usable for both quasi-zero (i.e., the French sites) and positive values (Indian site) of ponded depth on the infiltration surface.

3. Results and discussion

3.1. Calibration and Laboratory testing

Each infiltrometer had a unique calibration function between the visual readings of the water column heights and the corresponding voltage recorded during the emptying of the Mariotte bottle (Table 2). All transducers provided a nearly linear relationship between the voltage output and the heights of the water columns; as an example, $R^2 = 1.0$ for the calibration relationship collected using Infiltrator #3 (Figure 4, Table 2). They also had nearly identical values of the calibration multiplier ranging from 4.32×10^{-3} and 4.36×10^{-3} V/mm H_2O , while, as also noted by Ankeny (1992), the intercept yielded

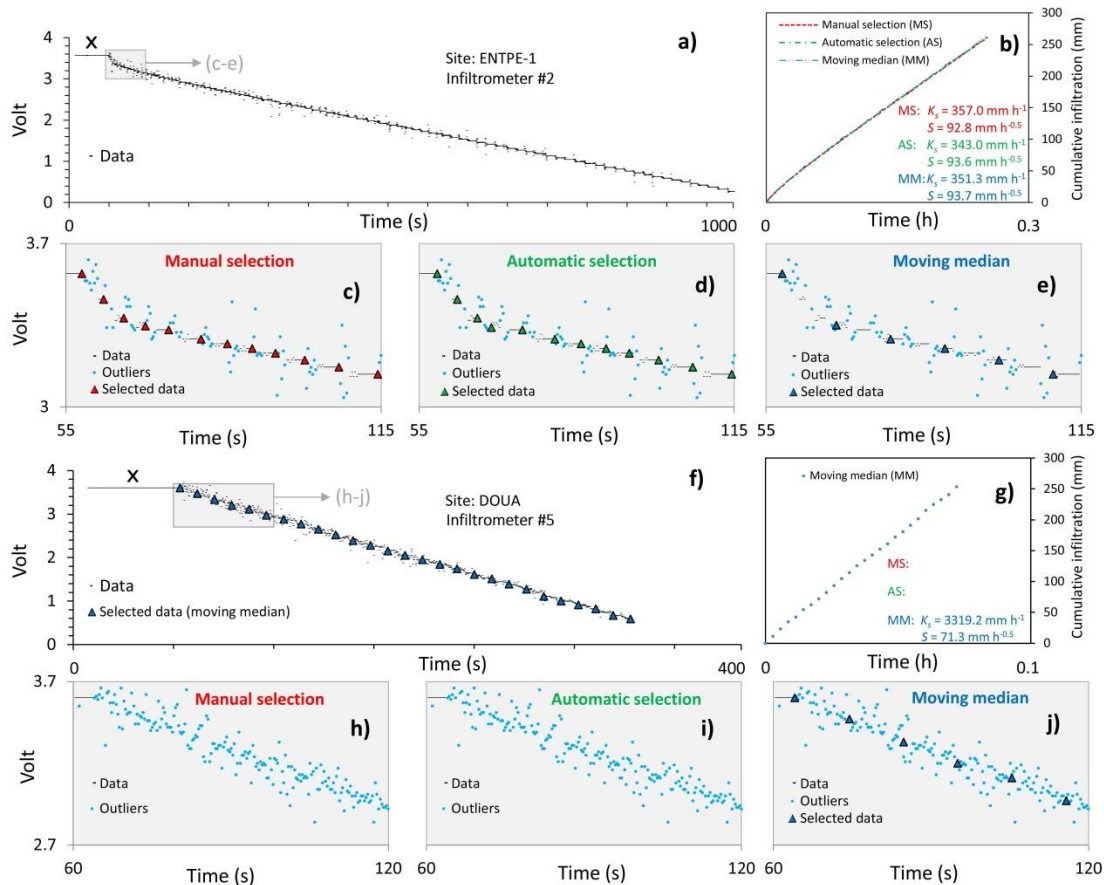


Figure 6. Examples of transducer output for (a) stair-like data and (f) a rapid infiltration process. Subpanels c-e present close views of the transducer readings reported in the gray rectangle of subpanel a and subpanels h-j show close views of the readings reported in the gray rectangle of subpanel f. Note that the manual and automatic procedures could not be applied to treat the raw data in case of rapid infiltration process (h and i) owing to an uninterrupted air bubbling that spoiled the transducer readings. (b and g) Determined cumulative infiltration amounts. The BEST-slope deduced S and K values are also reported. Note that the Mariotte bottles were filled with tap water and then activated through lifting the pistons, at which time data acquisition began. Then, the infiltration experiments started when the plastic films were removed. This procedure facilitated accurate data acquisition from the beginning of the run, with a constant transducer output during the first seconds of the experiments (x).

more variable values ranging from 0.328 and 0.390 mm. Nonetheless, while the calculation of the water levels is affected by the intercept value, the calculation of the water volume change between readings is independent from this parameter. However, the intercept value is still useful to exclude the water levels measured below the zero of the rule from the calculation of the water volumes, as the internal geometry of the Mariotte bottles changes below this level (Figure 2a). In the laboratory, the accuracy of the three procedures to treat the transducer output (i.e., manual selection, automatic selection and moving median) was evaluated through a comparison between recorded and measured cumulative flow data. All procedures yielded small errors (Table 3), suggesting that the ten infiltrimeters had good accuracy when measuring water flow. More specifically, the three procedures yielded RMSD ranging between 0.41 and 3.06 mm, Er between 0.28 and 2.06%, and $Er(I_{tot})$ between 0.06 and 1.76%. The three procedures did not yield significantly different errors (Table 3 and Figure 5). This result suggests that adopting a simplified procedure to treat the

transducer output, such as a moving median, does not negatively affect determination of flow data. In addition, the laboratory experiments, with a quasi-constant head of water maintained inside a cylinder, allowed us to test the infiltrimeters with a similar set-up to that one used on the field, thus increasing our confidence in the field measurements.

3.2. Field testing

3.2.1. Optimum case and peculiarities

Cumulative infiltration into an unsaturated porous medium typically exhibits a concave shape as a function of time, due to a decreasing hydraulic gradient as the wetting front moves away from the source and the influence of capillarity decreases (Xu et al., 2012). As flow rates approach steady state, cumulative infiltration becomes approximately linear with time (Angulo-Jaramillo et al., 2016). An example of this behavior is depicted in Figure 6a-e. In this example, the measured infiltration rates

Table 3. Minimum (Min), maximum (Max), mean, and coefficient of variation (CV) of the root mean squared differences, RMSD (mm), relative error, Er (%), and relative error, $|Er(I_{tot})|$ (%), of the total cumulative flow, I_{tot} (mm), for the three procedures to treat the transducer output. Sample size for each procedure, N = 10.

Error	Data treatment	Min	Max	mean	CV (%)
RMSD	Manual selection	0.41	3.06	1.60 A	48.3
	Automatic selection	0.46	2.66	1.52 A	50.9
	Moving median	0.81	2.73	1.71 A	41.2
Er	Manual selection	0.28	2.06	1.06 A	48.2
	Automatic selection	0.31	1.83	1.02 A	50.5
	Moving median	0.52	1.77	1.11 A	40.5
$ Er(I_{tot}) $	Manual selection	0.11	1.41	0.79 A	47.8
	Automatic selection	0.29	1.76	0.86 A	53.3
	Moving median	0.06	1.60	0.86 A	63.9

For a given variable, means followed by the same letter are not significantly different according to a paired, two-tailed t-test ($P < 0.05$).

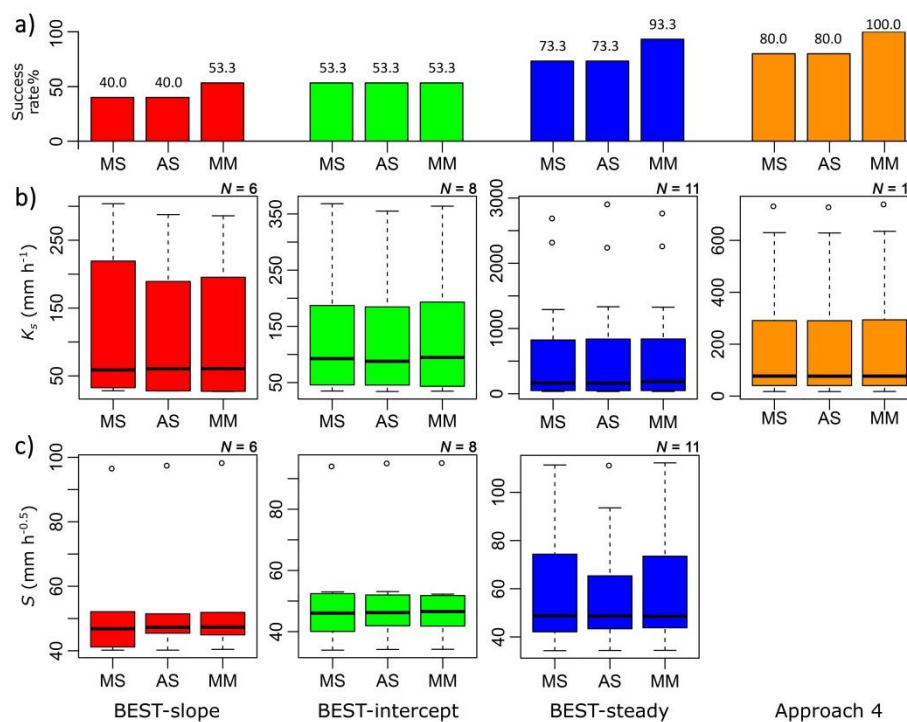


Figure 7. (a) Comparison between the success rates obtained for the three data treatments (i.e., manual selection, MS, automatic selection AS, and moving median, MM), and the four methods for estimating the hydrodynamic parameters (i.e., BEST-slope, BEST-intercept, BEST-steady and Approach 4). Box plots of the (b) saturated soil hydraulic conductivity, K_s (mm h⁻¹), and (c) soil sorptivity, S (mm h^{-0.5}), pairs data for the different scenarios. The sample size (N) for each box plot is also reported.

3.2.2. High flow rate experiments

For six out of fifteen experiments, the infiltration processes were entirely dominated by the influence of preferential flow paths, with infiltration rates ranging between 1529.8 and 5215.1 mm h⁻¹ (as estimated by the moving median approach). In such circumstances, we distinguished two different scenarios depending on the rapidity of the process. In three cases (first scenario), one at the ENTPE-1 site and two at the DOUA site, we measured infiltration rates equal or lower than 3159.3 mm h⁻¹ (Table 4). Still, the rapid infiltration process and the high measured infiltration rates did not cause uninterrupted bubbling within the Mariotte bottle. Therefore, the emptying process was characterized by the typical stepwise drop of water level in the reservoirs, yielding the same kind of stair-like output reported previously (Figure 2c and Figure 6a), and all the three procedures to treat the transducer output were successfully applied. However, the influence of preferential flow paths on the infiltration processes made it impossible to evaluate any effect of the capillary flow. Obviously, in such condition the use of transient models to fit infiltration data was inappropriate, and BEST-slope and BEST-intercept failed to provide S and K_s values (Lassabatere et al., 2019b). Three other experiments at the DOUA sites yielded even higher infiltration rates, ranging from 3496.3 and 5215.1 mm h⁻¹ (second scenario). Under these conditions, the manual and automatic procedures to treat the raw data could not be applied owing to the rapid emptying of the Mariotte bottle causing an uninterrupted air bubbling that spoiled the transducer readings (Figure 6h and i; also discussed in Di Prima et al., 2016). On the contrary, the application of a moving median successfully revealed the underlying trend of the transducer output with time (Figure 6f and j), thus allowing cumulative infiltration to be determined (Figure 6g). It also should be noted that, when the infiltration process was mainly driven by gravity and cumulative infiltration curves were near-linear (Lassabatere et al., 2019b), BEST-slope and BEST-intercept failed to provide S and K_s estimates, while BEST-steady was successfully applied. Indeed, according to Bagarello et al. (2014), BEST-steady does not

require data from the transient stage of the run but rather relies solely on the regression analysis of the final few cumulative infiltration depths. This particular algorithm avoided the uncertainties due to the linearity of the cumulative infiltration, which can obscure the distinction between the early- and late-time infiltration processes (Di Prima et al., 2018).

3.2.3. Improved description of the transient phase

The hypothesis of a better description of the transient phase when using the automatic infiltrometers was investigated through a comparison between the cumulative infiltration curves obtained from transducer output and discretized curves having the same increments as manually pouring water volumes into the containment ring. In the reported example (Figure 8), the infiltration reached steady state early (i.e., within the first 0.03 h) and only one discretized data point occurred within the transient flow regime. As a consequence, the transient infiltration models in BEST-slope and BEST-intercept could not be fitted to the discretized data. Conversely, the high-resolution cumulative infiltration curve obtained from the transducer output captured 14 points during the transient state, allowing for the BEST-slope (Figure 8c) and BEST-intercept algorithms to be fitted. In some cases, too few points could be identified for the description of the transient state. Such a problem occurred at the ENTPE-1 site, likely due to the high local initial soil water content there (Table 1). In addition to this example, BEST-slope also failed in two cases at the ENTPE-2 site whereas BEST-intercept was successfully applied; consequently, the former method had the lowest success rate (Figure 7). This shortcoming was already investigated in several investigations (e.g., Castellini et al., 2018; Di Prima et al., 2018). More specifically, when the early- and late-time infiltration stages greatly differ in terms of infiltration rates, the strong concavity of cumulative infiltration results in an overestimation of soil sorptivity. Such overestimations result in negative values for K_s , as already suggested by Yilmaz et al. (2010).

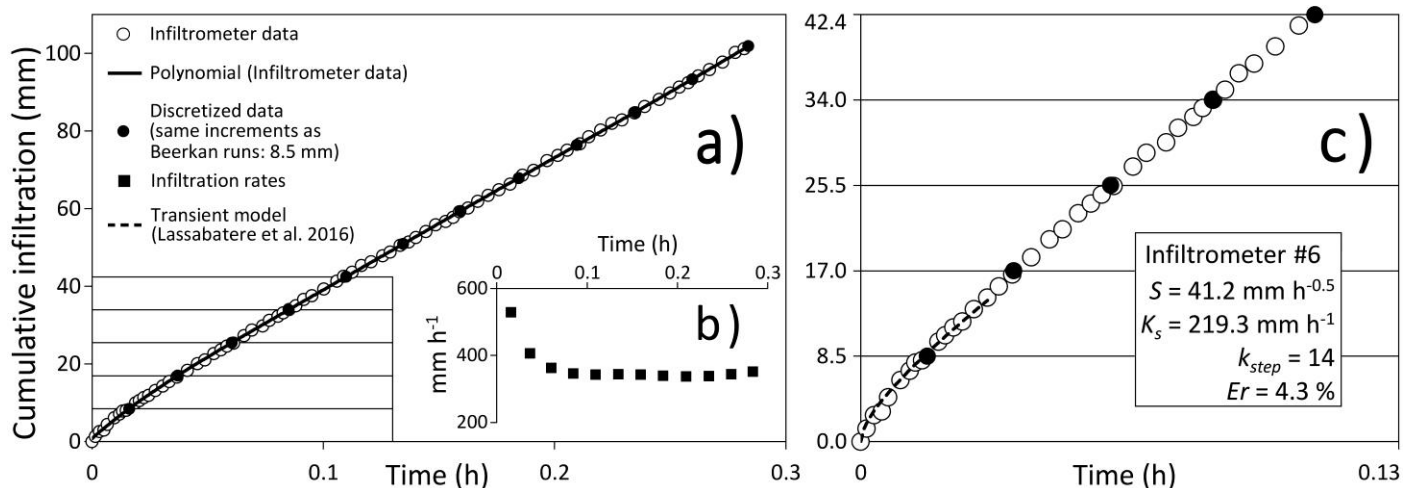


Figure 8. (a) Comparison between cumulative infiltration curves obtained from transducer output (open circles \circ) and discretized data (solid circles \bullet). The solid line is the polynomial function used to model the discretized data with the same increments as manually collected infiltration curves, i.e., 8.5 mm ("Beerkan-like data"). (b) Infiltration rates of the discretized data. (c) Detailed view of the early-time infiltration stage. The dotted line is the fitted cumulative infiltration model to the transient infiltration data. k_{step} is the number of datapoints used to fit the model.

3.2.4. Water repellent soils

The first obvious advantage in using automatic infiltrometer in case of water repellent soils is that data collection is automated and it does not require any further manipulation by the user once the device is installed. Therefore, tests can be successfully (and simultaneously) performed even if water repellency impedes infiltration and causes long testing durations (Alagna et al., 2018). In addition, the automatic infiltrometer used in this investigation was capable of maintaining a small water head on the soil surface, which helps to prevent excessive positive pressure from overcoming the soil water repellency (Nyman et al., 2010). For one experiment at the ENTPE-1 site, this experimental approach was useful to signal the occurrence of soil water repellency, as identified by cumulative infiltration having a convex curve shape (Di Prima et al., 2017). The cumulative infiltration data in that instance yielded a negative value for the intercept of the regression line fitted to the data points describing steady-state conditions (e.g., Alagna et al., 2018; Di Prima et al., 2019, 2017; Lozano-Baez et al., 2018). This circumstance led to the failure of all the BEST-algorithms (Lassabatere et al., 2019a); only Approach 4 provided an estimate of K_s . More specifically, BEST-slope and BEST-intercept failed because both algorithms required fitting transient models to early infiltration data that must be concave instead of convex as determined by soil water repellency. The BEST-steady algorithm avoids most problems associated with the use of the transient infiltration data, yet still estimates meaningless K_s data in case of negative intercept values. On the other hand, Approach 4 by Stewart and Abou Najm (2018) differs by the term expressing steady-state condition, considering exclusively the final infiltration rate, i.e., the slope of regression line fitted to the last data points of the cumulative infiltration. The exclusive use of this term allowed to consider only the final stage of the infiltration process, i.e., when the

water repellency had diminished or no effect on infiltration. Therefore, we suggest to use steady state methods, such as Approach 4, in case of water repellent soils (Angulo-Jaramillo et al., 2019). This example also illustrates that, when the physics of infiltration change, as in the case of water infiltration into water repellent soils, all the BEST methods are questionable (Bauters et al., 2003).

3.3. Comparison with the prototype

We also compared the cumulative infiltrations curves collected using the new infiltrometers with those measured by the prototype proposed by Di Prima (2015) on different soils analyzed during previous field campaigns (Di Prima, 2015; Di Prima et al., 2017, 2016). Figure 9 depicts a comparison between 45 curves collected with the prototype (Figure 9a) versus the curves collected with new infiltrometers at the ENTPE-1, ENTPE-2 and DOUA sites (Figure 9b). The mean value of the cumulative infiltration intervals, ΔI , decreased from 4.65 mm with the original prototype to 2.15 mm with the new version (Figure 9c). Therefore, the new infiltrometers had more than twice the resolution (i.e., shorter increments between readings) of the prototype. Returning the example shown in Figure 8, the updated version of the automated infiltrometer provided 14 measurements during the transient regime (Figure 8c), whereas the prototype would only have the capability to capture 3-4 points. Accurately modeling the transient state requires a minimum of five measurements (Angulo-Jaramillo et al. 2019), meaning that the prototype system would be inadequate in that scenario. At the same time, the new devices were able to collect measurements for longer durations (and greater cumulative infiltration amounts) due to their larger storage capacity. Thus, compared to the prototype system the new version of the infiltrometer can generate more data points during both transient and steady-state flow regimes.

Table 5. Results of the single- and double-ring infiltration experiments.

Method	Water depth (mm)	Steady infiltration rate (mm h^{-1})	K_s (mm h^{-1})
Single-ring	25	105.8	43.6
	50	80.5	30.6
	75	73.3	25.8
Double-ring	25	22.7	22.7
	50	22.5	22.5
	75	15.0	15.0

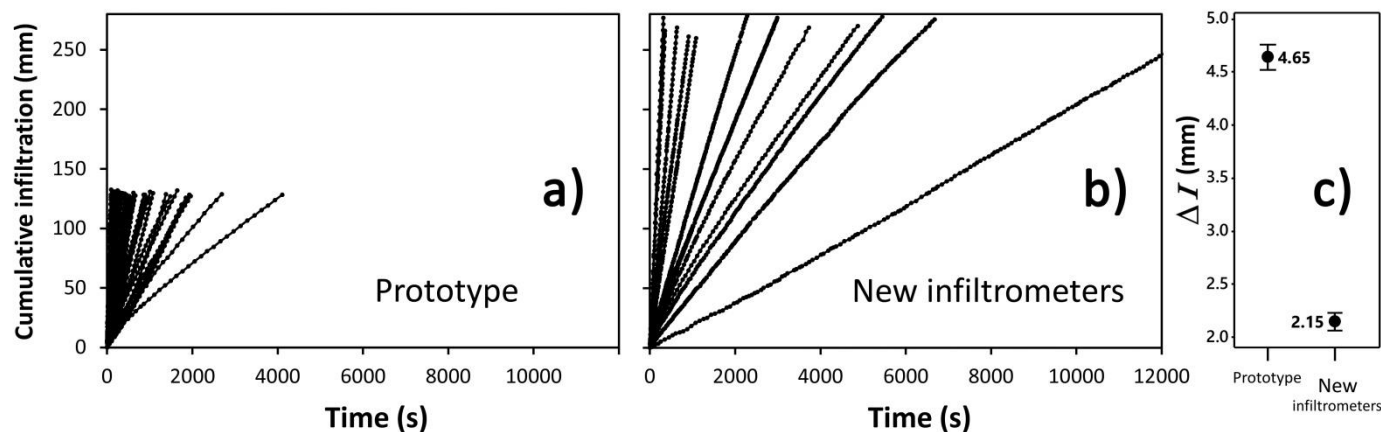


Figure 9. Comparison between cumulative infiltration curves collected with (a) the prototype proposed by Di Prima (2015) on different soils analyzed during previous field campaigns (Di Prima, 2015; Di Prima et al., 2017, 2016), versus (b) the curves collected with new infiltrometers at the ENTPE-1, ENTPE-2 and DOUA sites. Subpanel c displays the interval plots with the mean values of the cumulative infiltration intervals, ΔI (mm), and the 95% confidence interval bars. Individual standard deviations were used to calculate the intervals.

3.4. Application of the proposed device to double-ring measures

An automatic infiltrometer constructed at the Anand Agricultural University was used to run both of the single- and double-ring infiltration experiments. K_s values ranged between 15.0 and 105.8 mm h⁻¹ (Table 5). The different experimental setups, including multiple imposed water depths (25, 50 and 75 mm), showed the versatility of the device to execute experiments with multiple positive water heads, such as the one requested for the two- or multiple-ponding-depth approaches (Reynolds and Elrick, 2002b). For the double-ring experiments, the use of the infiltrometer to maintain the water level in the inner ring improved monitoring of the infiltration process while reducing the amount of effort needed to maintain a constant depth of water in both rings (Lai and Ren, 2007). The main advantage of using the automated infiltrometer in this scenario was its simplicity, in that it allowed a single operator to carry out the field experiments. In addition, the limited cost of the device means that it can contribute to more widespread applications of accurate and automated infiltration rates measurements, even when combined with cumbersome experiments such as the double-ring infiltrometer.

3.5. On the advantage of multiple infiltration experiments

The ability of the proposed instrumentation package to automatically collect data from up to ten infiltrometers working

simultaneously, i.e., when using ten infiltrometers connected to two data acquisition systems, was tested at the ENTPE-1 site (Figure 10). Such a protocol had many advantages. Indeed, ten replicates enabled the identification of specific runs, revealing either the effect of preferential flow (e.g., Figure 10b, run n. 10) or, on the contrary, the impedance of flux owing to water repellency (e.g., Figure 10b, runs n. 4 and 8). In addition, ten replicates should be appropriate to obtain representative mean values of soil hydrodynamic parameters at the field scale (Reynolds and Elrick, 2002a; Verbist et al., 2010). This protocol can help to overcome uncertainties in the hydraulic characterization of highly heterogeneous soils.

The new instrumentation package may constitute a valuable tool for the application of the Beerkan multi-runs procedure proposed by Lassabatere et al. (2019a), which consists in carrying out ten Beerkan infiltration experiments along a transect. The use of the automatic infiltrometers in this protocol may both provide sufficient water supply to reach steady state and provide measurement resolution needed to improve the description of the transient state. These advances allow the user to obtain more accurate estimates of soil hydraulic parameters, while also reducing the amount of effort needed to run multiple experiments.

4. Summary and conclusions

In this investigation we designed and manufactured a set of ten devices that automatically provide water at a constant head and record the resulting infiltration rates. The design of the

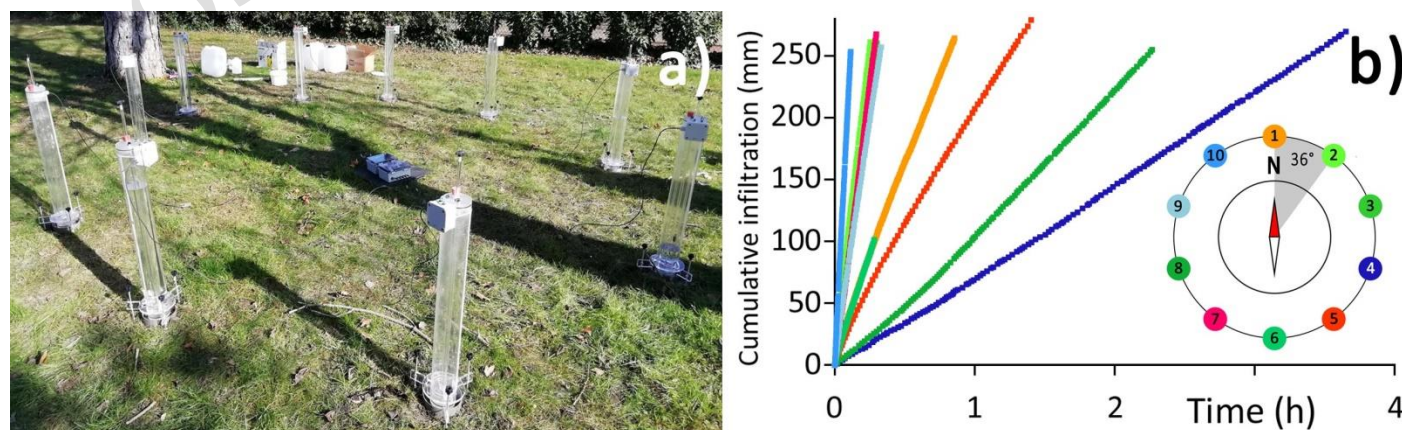


Figure 10. (a) Experimental setup consisting of ten infiltrometers working simultaneously and connected to two data acquisition systems, and (b) measured cumulative infiltration curves.

devices was improved over a previously presented prototype in terms of reservoir capacity (which controls the duration of the test), diameter of the air entry tube (which controls the measurement resolution and corresponding accuracy of infiltration measurements), and number of infiltrometers that can be simultaneously operated (here up to ten at one time). We also proposed a new algorithm for the automatic processing of the transducer readings, which substantially reduced the amount of work necessary to analyze the raw data. We encourage the readers to check the website bestsoilhydro.net for the latest updates, and also to download: Arduino sketches, electronic schemes, codes for data treatment, lists of components, models for 3D printing and laser cutting projects.

The devices were firstly tested in the laboratory and then on four different experimental sites under specific and challenging field conditions, such as highly permeable, slightly sorptive and water repellent conditions. The field campaigns highlighted the ease of use of the devices when performing either single-ring or double-ring infiltration experiments. The new instrumentation package provided in this study allows the user to intensively measure soil infiltration rates, with the capability of automatically recording multiple experiments. Automated measurements also facilitate better detection of preferential flow and soil water repellency conditions in the field.

Author Contributions

P. Concialdi and S. Di Prima realized the devices, outlined the investigation and carried out the experimental activity in France. H. Bhanderi realized the device and carried out the experimental activity at the Anand Agricultural University. L. Lassabatere coded the algorithm in Scilab for the automatic treatment of the transducer output. All authors contributed to discussing the results and writing the manuscript.

Acknowledgements

The authors wish to thank the Lyon city Field Observatory for Urban Water Management (OTHU), the Department of Agricultural, Food and Forest Sciences of the University of Palermo (Italy), and Pier Nicola Labate and Andrea Melis from the laboratory FabLab UniSS of the University of Sassari (Italy) for technical and scientific support. S.D.P. also thanks labandadipalermo.it for their contribution to keep the spirit up.

Funding

This work was supported through the INFILTRON Project (ANR-17-CE04-0010, Package for assessing infiltration & filtration functions of urban soils in stormwater management; <https://infiltron.org/>) funded by the French National Research Agency (ANR). Funding was also provided in part by i) the Virginia Agricultural Experiment Station and the Hatch Program of the National Institute of Food and Agriculture, U.S. Department of Agriculture, ii) the European Regional Development Fund (ERDF) and the Italian Ministry of Education, University and Research (MIUR) through the “Programma Operativo Nazionale (PON) Ricerca e Innovazione 2014-2020 (Linea 1 - Mobilità dei ricercatori, AIM1853149, CUP: J54I18000120001), and iii) the University of California – Davis Agricultural Experiment Station.

References

- Alagna, V., Iovino, M., Bagarello, V., Mataix-Solera, J., Lichner, L., 2018. Alternative analysis of transient infiltration experiment to estimate soil water repellency. *Hydrological Processes*. <https://doi.org/10.1002/hyp.13352>
- Angulo-Jaramillo, R., Bagarello, V., Di Prima, S., Gosset, A., Iovino, M., Lassabatere, L., 2019. Beerkan Estimation of Soil Transfer parameters (BEST) across soils and scales. *Journal of Hydrology* 576, 239–261. <https://doi.org/10.1016/j.jhydrol.2019.06.007>
- Angulo-Jaramillo, R., Bagarello, V., Iovino, M., Lassabatere, L., 2016. *Infiltration Measurements for Soil Hydraulic Characterization*. Springer International Publishing.
- Ankeny, M.D., 1992. *Methods and theory for unconfined infiltration measurements*. SSSA special publication series (USA) 123–141.
- Ankeny, M.D., Kaspar, T.C., Horton, R., 1988. Design for an Automated Tension Infiltrometer. *Soil Science Society of America Journal* 52, 893. <https://doi.org/10.2136/sssaj1988.03615995005200030054x>
- Ankeny, M.D., Prieksat, M.A., Kaspar, T.C., Noh, K.M., 1993. FLOWDATA: Software for Analysis of Infiltration Data from Automated Infiltrometers. *Agronomy Journal* 85, 955–959. <https://doi.org/10.2134/agronj1993.00021962008500040030x>
- Bagarello, V., Di Prima, S., Iovino, M., 2014. Comparing Alternative Algorithms to Analyze the Beerkan Infiltration Experiment. *Soil Science Society of America Journal* 78, 724. <https://doi.org/10.2136/sssaj2013.06.0231>
- Bauters, T.W.J., Steenhuis, T.S., DiCarlo, D.A., Nieber, J.L., Dekker, L.W., Ritsema, C.J., Parlange, J.Y., Haverkamp, R., 2003. Physics of hydrophobic soils. *Soil Water Repellency: Occurrence, Consequences, and Amelioration* 215–224. <https://doi.org/10.1016/B978-0-444-51269-7.50022-9>
- Bouarafa, S., Lassabatere, L., Lipeme-Kouyi, G., Angulo-Jaramillo, R., 2019. Hydrodynamic Characterization of Sustainable Urban Drainage Systems (SuDS) by Using Beerkan Infiltration Experiments. *Water* 11, 660. <https://doi.org/10.3390/w11040660>
- Braud, I., Desprats, J.-F., Ayrat, P.-A., Bouvier, C., Vandervaere, J.-P., 2017. Mapping topsoil field-saturated hydraulic conductivity from point measurements using different methods. *Journal of Hydrology and Hydromechanics* 65. <https://doi.org/10.1515/johh-2017-0017>
- Casey, F.X.M., Derby, N.E., 2002. Improved design for an automated tension infiltrometer. *Soil Sci. Soc. Am. J.* 66, 64–67.
- Castellini, M., Di Prima, S., Iovino, M., 2018. An assessment of the BEST procedure to estimate the soil water retention curve: A comparison with the evaporation method. *Geoderma* 320, 82–94. <https://doi.org/10.1016/j.geoderma.2018.01.014>
- Constatz, J., Murphy, F., 1987. An Automated Technique for Flow Measurements from Mariotte Reservoirs. *Soil Science Society of America Journal* 51, 252. <https://doi.org/10.2136/sssaj1987.03615995005100010051x>
- Decagon, 2014. *Minidisk Infiltrometer User's Manual*. Decagon Devices, Inc., Pullman, USA 24.
- Di Prima, S., 2015. Automated single ring infiltrometer with a low-cost microcontroller circuit. *Computers and Electronics in Agriculture* 118, 390–395. <https://doi.org/10.1016/j.compag.2015.09.022>
- Di Prima, S., 2014. A new automated single ring infiltrometer for Beerkan infiltration experiments [https://www.youtube.com/watch?v=2nok8MJWV9s].
- Di Prima, S., Bagarello, V., Angulo-Jaramillo, R., Bautista, I., Cerdà, A., del Campo, A., González-Sanchis, M., Iovino, M., Lassabatere, L., Maetzke, F., 2017. Impacts of thinning of a Mediterranean oak forest on soil properties influencing water infiltration. *Journal of Hydrology and Hydromechanics* 65, 276–286. <https://doi.org/10.1515/johh-2017-0016>
- Di Prima, S., Castellini, M., Abou Najm, M.R., Stewart, R.D., Angulo-Jaramillo, R., Winiarski, T., Lassabatere, L., 2019. Experimental assessment of a new comprehensive model for single ring infiltration data. *Journal of Hydrology* 573, 937–951. <https://doi.org/10.1016/j.jhydrol.2019.03.077>
- Di Prima, S., Concialdi, P., Lassabatere, L., Angulo-Jaramillo, R., Pirastru, M., Cerdà, A., Keesstra, S., 2018. Laboratory testing of Beerkan infiltration experiments for assessing the role of soil sealing on water infiltration. *CATENA* 167, 373–384. <https://doi.org/10.1016/j.catena.2018.05.013>
- Di Prima, S., Lassabatere, L., Bagarello, V., Iovino, M., Angulo-Jaramillo, R., 2016. Testing a new automated single ring infiltrometer for Beerkan infiltration experiments. *Geoderma* 262, 20–34. <http://dx.doi.org/10.1016/j.geoderma.2015.08.006>
- Haverkamp, R., Ross, P.J., Smettem, K.R.J., Parlange, J.Y., 1994. Three-dimensional analysis of infiltration from the disc infiltrometer: 2. Physically based infiltration equation. *Water Resour. Res.* 30, 2931–2935. <https://doi.org/10.1029/94WR01788>
- Klípa, V., Snehota, M., Dohnal, M., 2015. New automatic minidisk infiltrometer: design and testing. *Journal of Hydrology and Hydromechanics* 63. <https://doi.org/10.1515/johh-2015-0023>
- Lai, J., Ren, L., 2007. Assessing the Size Dependency of Measured Hydraulic Conductivity Using Double-Ring Infiltrometers and Numerical Simulation. *Soil Science Society of America Journal* 71, 1667. <https://doi.org/10.2136/sssaj2006.0227>
- Lassabatere, L., Angulo-Jaramillo, R., Soria Ugalde, J.M., Cuenca, R., Braud, I., Haverkamp, R., 2006. Beerkan estimation of soil transfer parameters through infiltration experiments—BEST. *Soil Science Society of America Journal* 70, 521. <https://doi.org/10.2136/sssaj2005.0026>
- Lassabatere, L., Di Prima, S., Angulo-Jaramillo, R., Keesstra, S., Salesa, D., 2019a. Beerkan multi-runs for characterizing water infiltration and spatial variability of soil hydraulic properties across scales. *Hydrological Sciences Journal* 64, 165–178. <https://doi.org/10.1080/02626667.2018.1560448>
- Lassabatere, L., Di Prima, S., Bouarafa, S., Iovino, M., Bagarello, V., Angulo-Jaramillo, R., 2019b. BEST-2K Method for Characterizing Dual-Permeability Unsaturated Soils with Pondered and Tension Infiltrometers. *Vadose Zone Journal* 18. <https://doi.org/10.2136/vzj2018.06.0124>

- Lozano-Baez, S.E., Cooper, M., Ferraz, S.F.B., Ribeiro Rodrigues, R., Pirastru, M., Di Prima, S., 2018. Previous Land Use Affects the Recovery of Soil Hydraulic Properties after Forest Restoration. *Water* 10. <https://doi.org/10.3390/w10040453>
- Madsen, M.D., Chandler, D.G., 2007. Automation and Use of Mini Disk Infiltrometers. *Soil Science Society of America Journal* 71, 1469. <https://doi.org/10.2136/sssaj2007.0009N>
- Milla, K., Kish, S., 2006. A low-cost microprocessor and infrared sensor system for automating water infiltration measurements. *Computers and Electronics in Agriculture* 53, 122–129. <https://doi.org/10.1016/j.compag.2006.05.001>
- Moret, D., López, M.V., Arrúe, J.L., 2004. TDR application for automated water level measurement from Mariotte reservoirs in tension disc infiltrometers. *Journal of Hydrology* 297, 229–235. <https://doi.org/10.1016/j.jhydrol.2004.04.003>
- Moret-Fernández, D., González, C., Lampurlanés, J., Vicente, J., 2012. An automated disc infiltrometer for infiltration rate measurements using a microflowmeter. *Hydrological Processes* 26, 240–245. <https://doi.org/10.1002/hyp.8184>
- Nyman, P., Sheridan, G., Lane, P.N.J., 2010. Synergistic effects of water repellency and macropore flow on the hydraulic conductivity of a burned forest soil, south-east Australia. *Hydrol. Process.* 24, 2871–2887. <https://doi.org/10.1002/hyp.7701>
- Prieksat, M.A., Ankeny, M.D., Kaspar, T.C., 1992. Design for an Automated, Self-Regulating, Single-Ring Infiltrometer. *Soil Science Society of America Journal* 56, 1409. <https://doi.org/10.2136/sssaj1992.03615995005600050013x>
- Reynolds, W., Elrick, D., 2002a. 3.4.3.2.b Pressure infiltrometer. In *Methods of Soil Analysis, Part 4, Physical Methods*, Dane JH, Topp GC (eds). SSSA Book Series, No. 5. Soil Sci. Soc. Am.: Madison, Wisconsin, USA 4, 826–836.
- Reynolds, W., Elrick, D., Youngs, E., 2002. 3.4.3.2 Ring or cylinder infiltrometers (vadose zone). In *Methods of Soil Analysis, Part 4, Physical Methods*, Dane JH, Topp GC (eds). SSSA Book Series, No. 5. Soil Sci. Soc. Am.: Madison, Wisconsin, USA 818–820.
- Reynolds, W.D., Elrick, D.E., 2002b. 3.4.3.3 Constant Head Well Permeameter (Vadose Zone), in: *Methods of Soil Analysis: Part 4 Physical Methods*, SSSA Book Series. Soil Science Society of America, Madison, WI, pp. 844–858. <https://doi.org/10.2136/sssabookser5.4.c33>
- Reynolds, W.D., Elrick, D.E., 1990. Ponded Infiltration From a Single Ring: I. Analysis of Steady Flow. *Soil Science Society of America Journal* 54, 1233. <https://doi.org/10.2136/sssaj1990.03615995005400050006x>
- Selker, J.S., Suter, J.D., Cuenca, R.H., Flugstad, B.A., Kelly, S.F., 2009. Tension infiltrometer enhancements with automated pneumatic control and more durable base plate: ENHANCED TENSION INFILTRMETER. *Water Resources Research* 45, n/a-n/a. <https://doi.org/10.1029/2008WR007075>
- Stewart, R.D., Abou Najm, M.R., 2018. A Comprehensive Model for Single Ring Infiltration II: Estimating Field-Saturated Hydraulic Conductivity. *Soil Science Society of America Journal* 82, 558–567. <https://doi.org/10.2136/sssaj2017.09.0314>
- Verbist, K., Torfs, S., Cornelis, W.M., Oyarzún, R., Soto, G., Gabriels, D., 2010. Comparison of single- and double-ring infiltrometer methods on stony soils. *Vadose Zone Journal* 9, 462–475. <https://doi.org/10.2136/vzj2009.0058>
- Xu, X., Lewis, C., Liu, W., Albertson, J.D., Kiely, G., 2012. Analysis of single-ring infiltrometer data for soil hydraulic properties estimation: Comparison of BEST and Wu methods. *Agricultural Water Management* 107, 34–41. <https://doi.org/10.1016/j.agwat.2012.01.004>
- Yilmaz, D., Lassabatere, L., Angulo-Jaramillo, R., Deneele, D., Legret, M., 2010. Hydrodynamic Characterization of Basic Oxygen Furnace Slag through an Adapted BEST Method. *Vadose Zone Journal* 9, 107. <https://doi.org/10.2136/vzj2009.0039>
- Zimmermann, B., Zehe, E., Hartmann, N.K., Elsenbeer, H., 2008. Analyzing spatial data: An assessment of assumptions, new methods, and uncertainty using soil hydraulic data: ANALYZING SPATIAL DATA. *Water Resources Research* 44, n/a-n/a. <https://doi.org/10.1029/2007WR006604>
- Zumr, D., Jeřábek, J., Klípa, V., Dohnal, M., Sněhota, M., 2019. Estimates of Tillage and Rainfall Effects on Unsaturated Hydraulic Conductivity in a Small Central European Agricultural Catchment. *Water* 11, 740. <https://doi.org/10.3390/w11040740>